Electronic Supplementary Material (ESI) for Nanoscale.

Supporting Information:

Characterising Porosity in Platinum Nanoparticles

Wenmiao Yu[1], Christopher Batchelor-McAuley,[1]* Yi-Chi Wang[2], Shouqi Shao[2], Sarah J Haigh[2], Simon M. Fairclough[2], Neil Young[3]* and Richard G. Compton[1]*

[1] Physical and Theoretical Chemistry Laboratory, Department of Chemistry, University of Oxford, South Parks Road, Oxford OX1 3QZ, United Kingdom

[2] School of Materials, University of Manchester, Oxford Road, Manchester M13 9PL, United Kingdom

[3] Department of Materials, University of Oxford, Parks Road, Oxford OX1 3PH, United Kingdom

* corresponding author email:
Christopher.Batchelor-McAuley@chem.ox.ac.uk
Neil.Young@materials.ox.ac.uk
Richard.Compton@chem.ox.ac.uk

Contents

Section 1: Average Nanoparticle Diameter Analysis and Cumulative Frequency

1.1 Average Nanoparticle Diameter

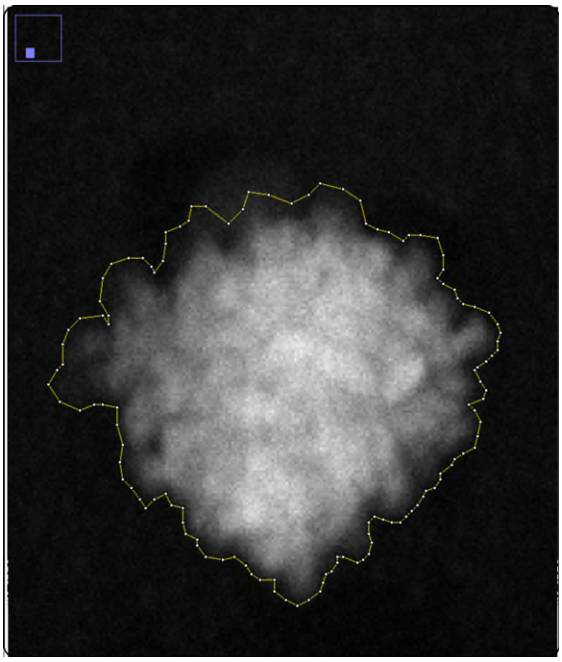

Figure SI 1.1 A representative HAADF-STEM image of a porous platinum nanoparticle, this image demonstrates the method used for measuring the effective diameter of the particle. The outline of the particle is traced out and the area contained by this shape is converted into an effective diameter ($A=\pi D^2/4$)

Due to the porous particles not being perfectly spherical it is important to outline how the average or effective particle diameter is measured, this is particularly relevant in this work as the particles image intensity is subsequently compared to that expected for a spherical laser ablated particle. In ImageJ, a tight-fit selection of the parameter of the particle is made as shown in Figure 1.1. From this projected nanoparticle area (A) the average diameter (d) was determined by:

d = sqrt(4A/pi)

1.2 Cumulative Frequency

Throughout this work size distributions are presented as relative cumulative frequency plots. The relative cumulative frequency gives a direct way of visualizing the fraction of the particles that are below a certain size limit. The relative cumulative frequency is equal to the cumulative frequency divided by the sample size.[1] The choice to use this method of visualizing the data is twofold. First, how data is visualized using size histograms depends on the used bin size. Second, by presenting the data as a fraction of the whole population it is straightforward to determine what fraction of the particles are

above a certain size limit; this is particularly useful in situations where the size distribution is not well described by a Gaussian curve. It is common for particle sizes to be approximately log-normally distributed and hence due to the positive skew on the distribution in some case large particles can form a significant fraction of the number population. In cases where the sample size is comparatively low visualizing this tail in the distribution using a size histogram can be more challenging.

The size histogram is related to the derivative of the relative cumulative frequency plot.

Section 2: Electron Tomography Reconstruction Details and Thresholding Data

The HAADF-STEM tomography was acquired on an FEI Titan G2 operated at 200 kV using beam current 100 pA, pixel size 0.138 nm, dwell time 10 us and tilting range from –72° to 76° with 2° increments. After acquisition, tilt series image stacks were aligned by cross-correlation to minimise inter-frame shift. TomViz software[2] was used to align tilt axis rotation and shift. TVM reconstruction[3] with 5 iterations was performed in TomViz to reconstruct the 3D tomogram. This procedure was applied to all 5 tilt series data sets.

As the specimen consists of only one element, a high intensity in the 3D tomogram is considered to represent a region contain platinum and a low intensity is attributed to pores inside the nanoparticle. Therefore, a hysteresis thresholding method[4] was applied to the 3D tomogram to segment regions containing Pt and allow quantification of the 3D surface area and particle density. Hysteresis thresholding requires two values to be chosen, a 'low threshold' value and a 'high threshold' value. These values are used to classify voxels to be part of the particle reconstruction volume if either of the following conditions is fulfilled: 1) the voxel intensity is higher than the 'high threshold' value; or 2) the voxel intensity is between the low and the high threshold values and connects any two voxels with intensities higher than high threshold value. This threshold method reduces the chance that reconstruction artefacts are included in the reconstruction as these are usually present on the edge of the reconstruction.

The high threshold value for all five reconstructions is chosen as 1.8 as a conservative estimate for the intensity of voxels containing Pt. The low threshold value is varied for each tomogram and is chosen to give a thresholded tomogram as demonstrated in Figure SI 2.1.

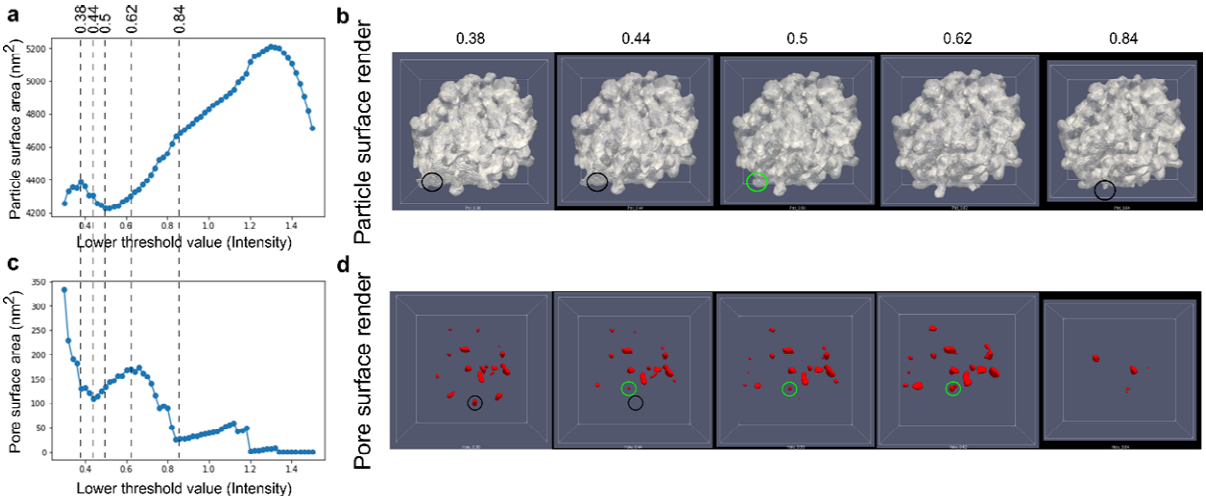

Figure SI 2.1 a) Particle surface area as a function of low threshold value from 0.3 to 1.5. b) Five surface renders of the particle area after applying thresholding with low threshold values corresponding to the dashed lines in a). c) Pore surface area as a function of low threshold value from 0.3 to 1.5. d) Five surface renders of the internal pore area after applying thresholding with low threshold values corresponding to the dashed lines in c). In b) and d), black circles highlight where there is considered to be an unphysical addition of particle surface. Green circles are where true features are missed.

Figure SI 2.1a shows the particle surface area and void surface areas plotted as a function of the choice of low threshold values from 0.3 to 1.5. Five surface renderings of the particle and voids at different low threshold values are shown Figure 1.1. Left to right the tomograms used low threshold values of 0.38, 0.44, 0.5, 0.62 and 0.84 respectively. When the low threshold value is too low (below 0.5), weak intensity artefacts are falsely classified as particle and the particle surface area is higher than its local minima. In addition, as more voxels are classified as particles, concave particle surfaces may be closed to form false voids (indicated by black circles in Fig SI 2.1 d) or small pores are falsely classified as particle regions (green circles in Fig SI 2.1 d). These false classifications lead to oscillations of the pore surface areas shown in Fig SI 2.1 c. At a low threshold value 0.84, the particle surface area is much higher than its local minima and pore surface area is much lower than its local maxima, this indicates that thresholding has caused "erosion" of the tomogram and internal voids. For this example particle, the low threshold value (0.5) for local minimum particle surface area is not the same as the threshold value (0.62) that results in local maximum void surface area. The values resulting from these two low threshold values are compared in Table SI 2.1. Thus the choice of low threshold value only results in a difference of 2% for the particle surface area quantification. The low threshold value, tomogram histogram, particle surface area, pore surface area and thresholded tomograms for all 5 reconstructions are shown in Fig SI 2.2.

SI Table 2.1. Quantification of the reconstruction shown in main text with two different low threshold values (0.5 and 0.65).

Threshold value	0.5	0.62	Difference of 0.62 comparing to 0.5 (%)
Particle volume	9246 nm^3	8666 nm^3	-6%
Pore volume	36 nm^3	50 nm^3	39%
Inscribed sphere volume	15260 nm^3	15055 nm^3	-0.1%
Particle surface area	4229 nm^2	4301 nm^2	2%
Equivalent particle surface area	2130 nm^2	2040 nm^2	-4%
Pore surface area	133 nm^2	170 nm^2	28%

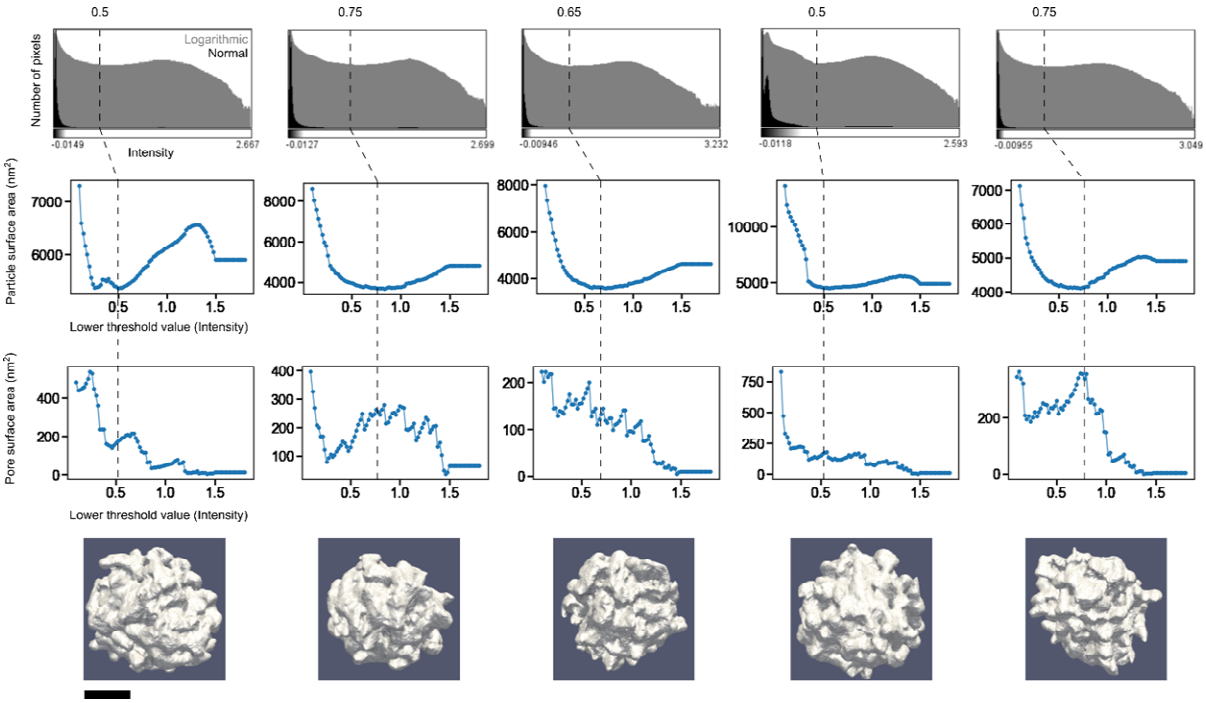

Fig SI 2.2. From top to bottom, tomogram intensity histogram, particle and pore surface area as a function of low threshold value and the thresholded tomogram. The leftmost column is the tomogram shown in the main text. Scale bar is 10 nm.

Section 3: High-Resolution Conventional Transmission Electron Microscopy of the Solid Laser Ablated Platinum Nanoparticles

The laser ablated solid Pt nanoparticle aggregates were characterised using High Resolution Transmission Electron Microscopy (HR-TEM), a representative image of the laser ablated particles is shown in Figure SI 3.1. For comparison a TEM image of the laser ablated solid Pt nanoparticle aggregates is presented in Figure 3 (of the main text).

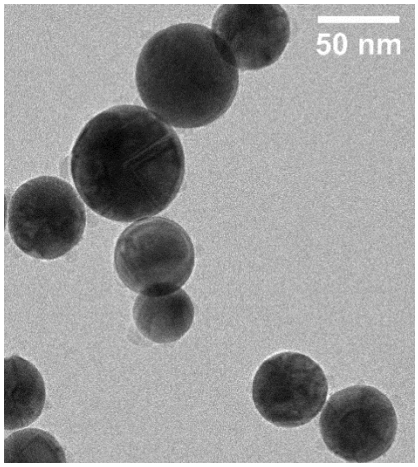

Figure SI 3.1 Representative HR-CTEM image of the laser ablated, solid PtNPs

The size and shape of the laser ablated nanoparticles was analysed using imageJ. Figure SI 3.2a) presents the corresponding particle size distribution, where the measured particle diameter has been plotted as a relative cumulative frequency. The average particle diameter was determined to be 53.1 ± 21 nm, from the measurement of 111 particles. The large uncertainty reflects the wide spread of nanoparticle sizes. Beyond having a wide size distribution another notable feature of the laser ablated particles is their regular shape and high sphericity. Figure SI 3.2b) plots the maximum and minimum Feret diameters for the nanoparticles; the strong correlation reflects their highly spherical nature.

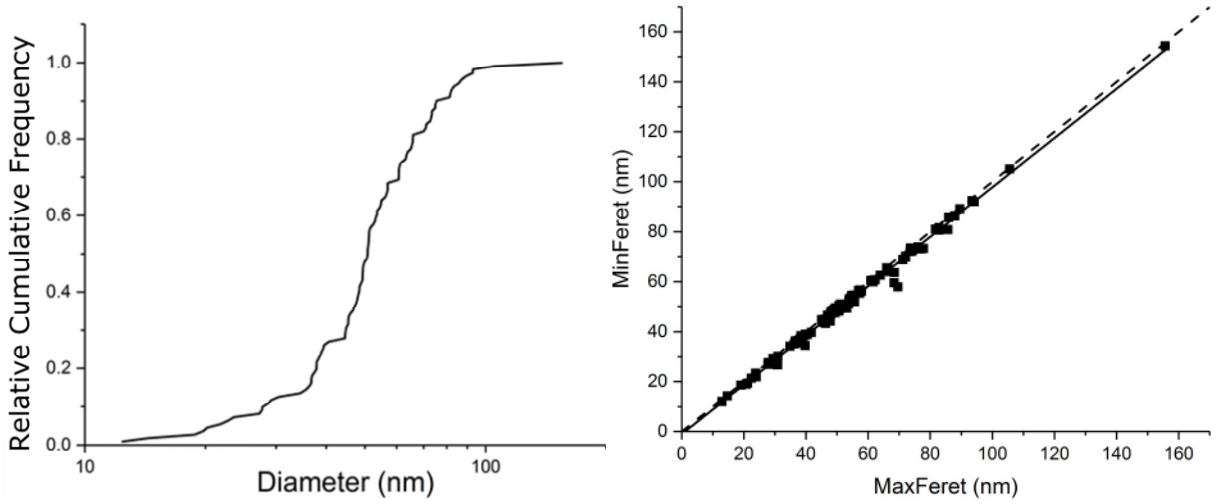

Figure SI 3.2 a) A plot of normalized cumulative frequency against particle diameter on a log scale for the laser ablated Pt nanoparticles with a mean diameter measured as 53.1 ± 21 nm (of 111 measurements) and b) a plot of minimum Feret diameter against maximum Feret diameter for laser ablated Pt NPs (111 particles measured from HR-TEM images), with a line of best fit through measurement points (solid black) and a line of gradient 1 (dashed black). The laser ablated particles have nearly perfect circular symmetry.

Section 4: HAADF-STEM Image Maximum Intensity and Background Correction

The maximum intensity is defined as the intensity of the point at the center of a PtNP. This value was determined by selecting the particle of interest and using the *Radial Profile* plugin in imageJ developed by P. Baggethun. The plugin produces a plot of normalized integrated intensities around concentric circles as a function of distance from the central in the selected circle. The sum of the pixel values around the circle is represented by the intensity at any given distance from the point (*r* (nm)). The intensity at *r* = 0 nm (the centre of the particle) is obtained from the plot, Figure SI 4.1 plots the raw (blue markers) measured maximum HAADF-STEM intensity as a function of the measured particle diameter.

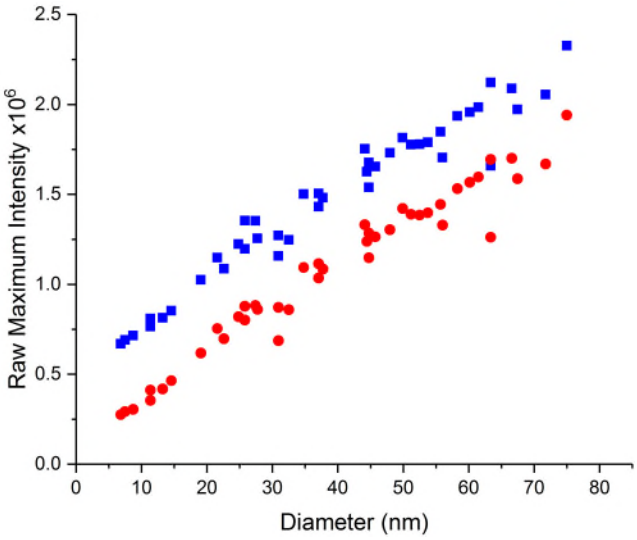

Figure SI 4.1 The measured maximum HAADF-STEM image intensity (arb units) for a series of laser ablated nanoaprticles plotted against their measured diamter. Blue markers represent the raw values and the Red markers represent the same data set once corrected for the background image intensity as expressed by equation 3.1.

Due to the non-zero background scattering the maximum image intensity required correcting where the value of $\text{Intensity}_{\text{bkg}}$ is measured on the same micrograph and the data corrected as follows:

$$\text{Intensity}_{\text{max}} = \text{Intensity}_{r=0} - \text{Intensity}_{\text{bkg}}$$

where $\text{Intensity}_{\text{bkg}}$ is the average intensity measured for the background and $\text{Intensity}_{\text{max}}$ is the background corrected maximum intensity value of the selected PtNP. All intensity values have arbitrary units.

Section 5: Integrated Particle Image Intensity, Raw Data

To attain a measure of the amount of platinum material contained in the porous nanoparticles the intensity of the 2D HAADF-STEM image was integrated across the entire nanoparticle structure. Figure SI 5.1 depicts example measured integrated image intensities for both the porous and solid (laser ablated) nanoparticles. Due to the laser ablated nanoparticles being denser their integrated image intensity is higher than that for an equivalently sized porous platinum nanoparticle structure. To attain a relative measure of the nanoparticle density a line of best fit for the solid data (on this semi-log plot) was used as a calibration line against which the intensity of the porous nanoparticle could be compared. The average diameter for the solid platinum nanoparticles was 53.1 ± 21 nm; consequently, although the solid platinum nanoparticles had a wide size distribution the population of particles with diameters below ca. 35 nm was comparatively low. Moreover, as evidenced by Figure 3 of the main text, for the larger particles their image intensity is significantly affected by beam attenuation. Consequently, the sample size of laser ablated spherical nanoparticles suitable for comparison with the 30 nm porous platinum nanoparticles was comparatively limed.

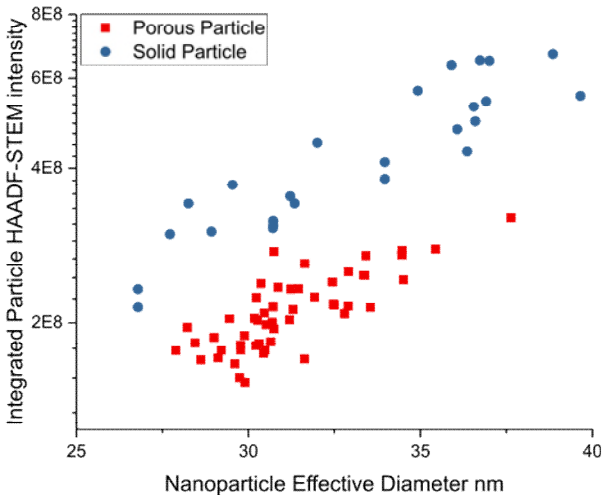

Figure SI 5.1: Comparison of the HAADF-STEM nanoparticle image integrated intensities as measured for the solid (blue) and porous(red) platinum nanoparticles.

Section 6: Integrated Particle Image Intensity Analysis, Simulation

This section explores the used method for estimating the overall particle density from the 2D HAADF-STEM images. This is achieved by using a simplified model of the porous platinum nanoparticles and simulating the HAADF-STEM image. These simulated images are then analysed in the same manner as the experimental data so as to yield insight into any systematic errors that may be incurred by the applied methodology.

6.1 Simulated HAADF-STEM Analysis

General Purpose Graphics Processing Units (GPGPU) are now widely available through cloud computing services, making the STEM simulation of larger nanoparticulate structures possible. The following simulations were undertaken on the Google Cloud Platform using a virtual computer instance with 4 CPUs, 15 GB of memory and with a single NVIDA Tesla P100. The system was running Debian GNU/Linux 9.6 with cuda 10.0. Scripts were written on Python 3.6 (Anconda, Auston TX). First, three dimensional idealized models of the nanoparticle were constructed calling on the use of HOOMD-blue[5, 6] for the production of random nanoparticle clusters using the hard particle monte carlo package.[7] Second, the HAADF-STEM image was simulated through the use of GPGPU enabled Prismatic software.[8, 9] All constructed models occupied a volume no greater than 40x40x40 nm^3, although the base of the model was always the same size the z height depended upon the simulated nanoparticle structure.

6.2 Spherical Particle Simulation

Figure SI 6.1 a) depicts an idealized 3D model of a spherical platinum nanoparticle (red diameter 25 nm) partially embedded into an amorphous carbon support (blue 40x40x5 nm). The platinum nanoparticle has been shifted off-axis by 20 degrees in both the x and y axis to avoid issues associated with electron channeling. To simulate the STEM image using the Prismatic software package this 3D model was divided into 400 constituent sub-models. The multislice method was used to simulate the HAADF-STEM TEM images and the used simulation parameters are chosen to be comparable (although not identical) to the physical specifications of the JEOL JEM-3000F TEM used for imaging in this work, i.e. beam energy 300 kV, aberration C3 $6x10^6$ Å, C5 $2x10^7$ Å but a probe-semi angle of 10 mrad. Furthermore, a slice thickness of 2 Å, a potential bound of 2 Å and a single frozen phonon were used as the simulation parameters. Figures SI 6.1 b) and c) depict the simulated bright field (0-3 mrad) and dark-field (>55 mrad) images of the 25 nm platinum particle. On average simulation times were less than 24 hours.

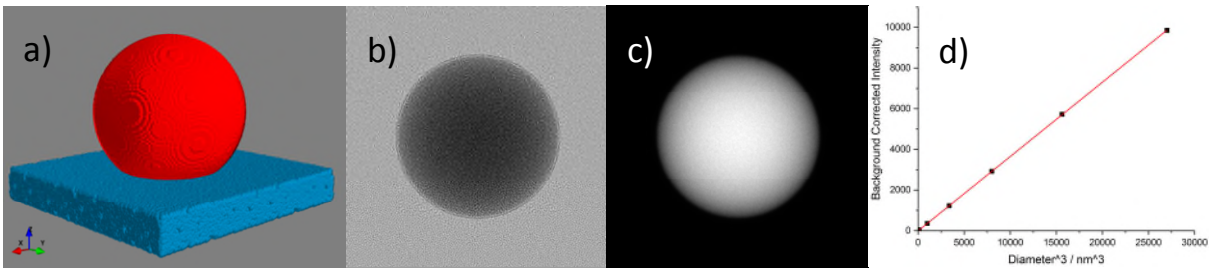

Figure 6.1: STEM simulation of a perfect 25 nm spherical particle. a) 3D rendering of the model b) simulated bright field image (0-3 mrad) and c) simulated dark-field image (>55 mrad). d) depicts the variation of the simulated image intensity (integrated across the entire particle) of the nanoparticle against the particle diameter cubed.

HAADF-STEM simulations of perfectly spherical particles in the size range of 5-30 nm were under taken. Figure SI 6.1 d) plots the simulated HAADF integrated particle image intensity against the particle diameter cubed. In this size limit the integrated image intensity scales essentially linearly with the volume of the material contained in the particle. Note although the particles used in the experimental study are larger than 30 nm in size, even with the use of a powerful GPGPU simulation of particles larger than approximately 30 nm in size is prohibitive on the basis of the required simulation times (>24 hours).

6.3 Porous Particle Simulation

To investigate the effect of the porous structure of a particle on the image intensity, a series of cluster particles were constructed. Here the particles were formed of small ideal truncated octahedra, these particles were initially formed into a perfect space filling *cubic* solid. Using the software package HOOMD-blue, the crystallites contained in these structures were numerically allowed to randomly move and re-orientate on the basis of a Monte Carlo simulation method. The applied dimensionless pressure used in the simulation allows control over the extent to which the cluster structure is able to expand and the individual clusters re-orientate. Note HOOMD-blue presently only allows numerical simulation in triclinic space, hence after the Monte Carlo simulation so as to ensure that all of the particles were of a comparable size and shape only crystallites whose centre was within 15 nm of the center of the simulation space were used to create the particle cluster models, thus enabled the production of quasi-spherical particles. Figure SI 6.2 shows three example particle cluster models formed of the smaller crystallites, where the crystallites have been allowed to randomly rearrange.

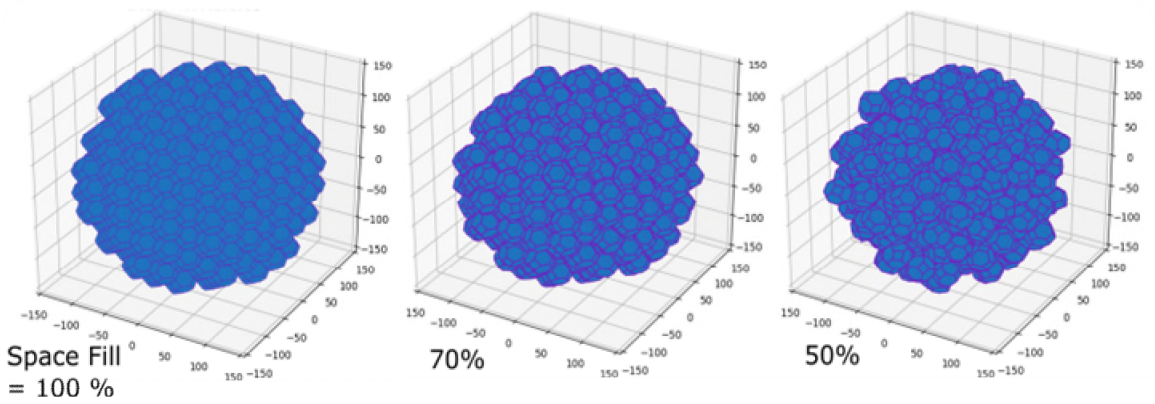

Figure SI 6.2: 3D redndered images of randomised cluster structure models, produced through the use of HOOMD-blue. By decreasing the used simulation dimensionless pressure it is possible to controllably create particle cluster structures with different percentage packing of the constituent particle. Lengths on the axis are given in Angstroms.

The space filling percentage of these models has been calculated on the basis of the percentage 'fill' of the core (central 10 nm radius) of the material, so that the 'roughness' of the outer particulate structure does not contribute to this measured value. As can be seen from the structures presented in figure 6.2, as the overall density of the particulate structure is decreased, the substituent crystallites become less aligned. Using this model construction method, two sets of HAADF-STEM simulations were produced for clusters with different overall densities and either formed from truncated octahedral containing 1289 or 4033 platinum atoms. Figure SI 6.3 depicts six representative simulated HAADF-STEM images of cluster particles with differing space fill factors.

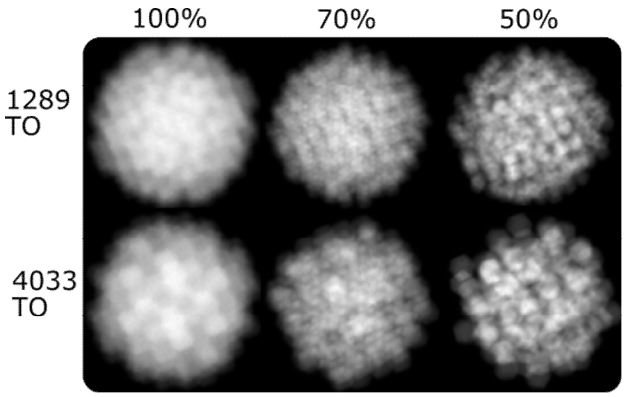

Figure SI 6.3 Simulated HAADF-STEM images of the model platinum nanoparticle clusters, with two different sizes of substituent crystallites (truncated octahedral 1289 and 4033 atoms per sub crystal) and with differing overall densities (space fill).

6.4 Simulated image intensity comparison

As the space fill or overall particle density decreases the particle image intensity correspondingly decreases. In order to use this decrease in image intensity to provide a measure of the particle density it is necessary to quantitatively compare these images to those attained for the idealized spherical particles. The question is 'what is the effective diameter of the cluster particles'? The reason this question is critical is that as shown from Figure SI 6.1 d) the particles integrated image intensity varies with the cube of its diameter (i.e. its volume). In this work as outlined in the SI section 1 the particles projected area is used to estimate the effective particle diameter. Once the diameter and the integrated image intensity of the particle has been measured the intensity is compared to that of a perfect sphere the ratio of the measured to expected particle image integrated image intensity is used as a measure of the particles overall density.

Figure SI 6.4 plots for these two series of simulated model cluster particles (1289 and 4033) the estimated density of the particle as attained from the procedure above involving the measurement of the image intensity against the model's known particle space filling. For both sets of simulated data the integrated image intensity normalized against that expected for a perfect sphere of equivalent diameter gives a reliable method for determining the overall density of the material. Note Figure SI 6.4 evidences to some extent that this used method marginally (3-5%) underestimates the density of the particle. This suggests a systematic error is incurred due in the ambiguity of defining an effective diameter of the particle.

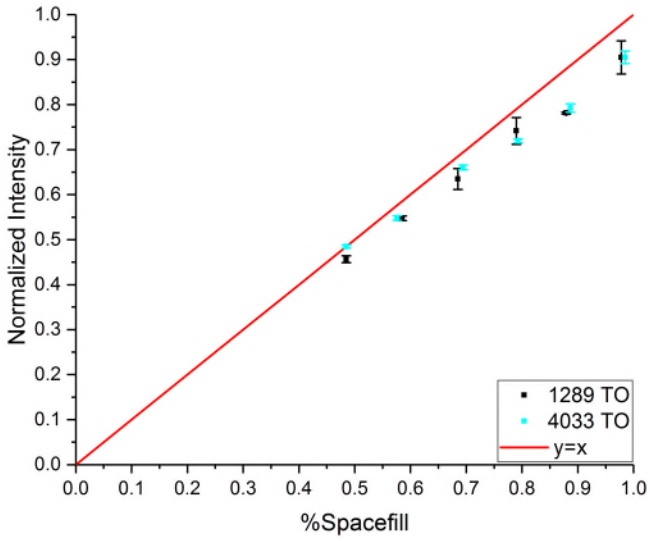

Figure SI 6.4: Analysis of the simulated HAADF-STEM images to give a measure of particles overall space fill or 'density' as measured from the resulting image plotted against the known density of the material used in the actual model.

This simplified simulation model evidences the validating of using the intensity of the experimentally measured HAADF-STEM images to yield an estimate of the particles space fill and to give insight into the extent to which the structure contains pores.

Section 7: Single Nanoparticle Electrochemical Surface Area Measurements

Submerging an Au microelectrode (10 µm diameter, potentiostated to +0.25V (vs MSE)) into a 6 pM suspension of 30 nm Pt nanoparticle clusters (diameters of 31 nm as determined by HR-TEM) in a non-buffered solution of 20 mM $NaNO_3$ in the presence of hydrogen leads to the observation of spikes in the measured current-time profile. In the presence of hydrogen in the solution phase the platinum nanoparticles become chemically modified by chemisorption and homolytic cleavage of the hydrogen on to the catalytic interface of the material. Figure SI 7.1 depicts a representative chronoamperogram where the Au microelectrode (the working electrode) has been held under potentiostatic control at a potential of +0.25 V vs MSE for 120 s. The spikes correspond to the arrival of individual Pt nanoparticle aggregates to the electrode surface, and the subsequent removal of hydrogen from the Pt interface upon electrical contact. As given by:

$$\mathrm{Pt-H} + \mathrm{OH^-} \leftrightarrow \mathrm{M} + e^- + \mathrm{H_2O}$$

To ensure only H_{upd} oxidation is studied a potential of +0.25 V vs MSE was selected to avoid any influence caused by the Pt catalysis of the HOR occurring at more negative potentials.[10]

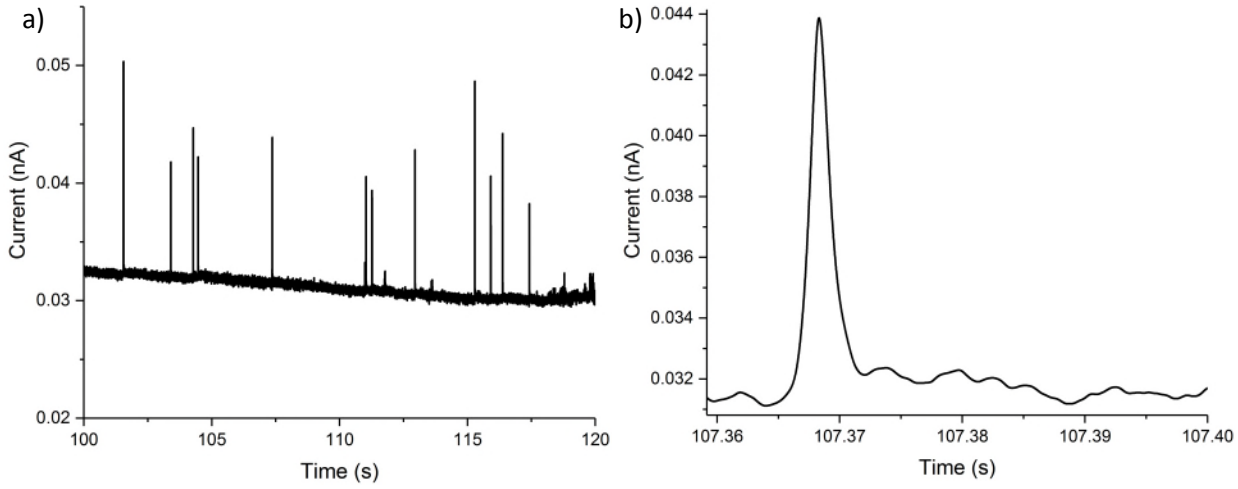

Figure SI 7.1 a) Sections of chronoamperograms of 6 pM 30 nm Pt nanoparticle aggregates in 20 mM $NaNO_3$ at an Au microelectrode with an applied potential of +0.25 V (vs MSE) and b) zoomed in images of the spikes from the sections above.

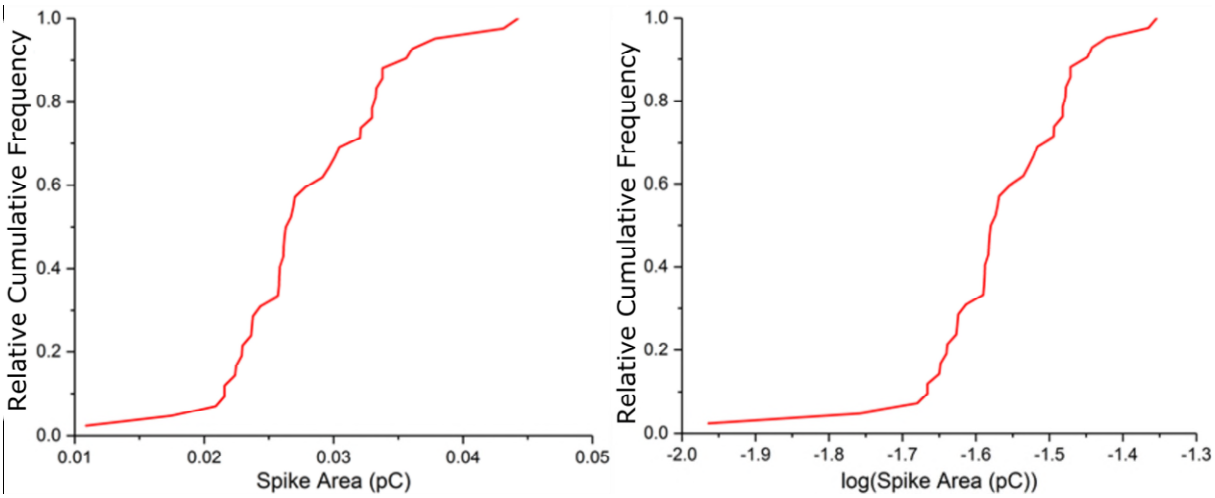

Figure SI 7.2 a) A plot of the normalized cumulative frequency against the spike area for the 30 nm Pt nanoparticle aggregates with a mean spike area calculated to be 0.028 pC (of 42 spike measurements) and b) a plot of the normalized cumulative frequency against the log(Spike Area).

By integrating the spike features the charge passed per nano-event can be measured. Figure SI 7.2 plots the relative cumulative frequency plots of the measured charge. The relative cumulative frequency gives a measure of the fraction of events that had a charge equal to or less than the value given on the x-axis. For instance from Figure SI 7.2 a) we can see that 30% of the spikes had a charge less than or equal to 0.024 pC. Similarly only 10% of the measured spikes had a charge greater than 0.036 pC. This charge per nano-event can be converted into an electrochemical surface area. If we assume that there is initially a monolayer coverage of hydrogen on the platinum surface and that upon impact all of the chemisorbed hydrogen is removed then we can relate the charge passed to the nanoparticle surface area. The lattice parameter for platinum is 0.392 nm, hence a Pt(100) surface has a surface density of 1.3×10^{19} atoms nm^{-2}. If we assume there is one chemisorbed hydrogen per platinum and that this hydrogen undergoes a one electron oxidation to a proton then we expect the charge associated with one monolayer of hydrogen to be 2.1 C m^{-2}. This value of 2.1 C m^{-2} is routinely used in the field of electrocatalysis to convert the measured electrochemical charge into an electrochemical surface area.[11] Hence, we can convert the measured charge for individual nano-events into electrochemical surface areas of individual impacting nanoparticles, as plotted in the inlay of Figure 5 in the main text.

An important assumption in the above is that we are removing a full monolayer of hydrogen. Direct evidence for the validity of this assumption is found in our previous work.[12] In this earlier article we demonstrated that if the same process is studied in the opposite direction, reductively (i.e. deposition of H_{upd} as opposed to its removal), then the same charge distribution is measured. This experimental

evidence strongly corroborates the assumption that we are removing a full monolayer of chemisorbed hydrogen.

Section 8: UV-Vis Measurements on the Platinum Nanoparticle Sol in the presence of Electrolyte

For UV−vis (Shimadzu UV1800 UV−Vis spectrophotometer) measurements, the stock mesoporous 30 nm PtNP suspension was diluted by a factor of 2 with ultrapure water to obtain absorbance in an analytically meaningful range. Both deuterium and halogen light sources were used, with the sample being scanned from 1100 to 190 or 236 nm. A broad surface plasmon peak just below 236.6 nm was observed, indicating the presence of 30 nm mesoporous PtNPs.

UV/Vis was used to determine the extent of agglomeration of the Pt nanoparticle aggregates in 20 mM $NaNO_3$ as a function of time when saturated with air, H_2 and N_2. UV/Vis spectra of 0.026 mg mL^{-1} 30 nm Pt nanoparticle aggregates in 20 mM $NaNO_3$ were taken every 5 minutes over a 60 minutes period, where the nanoparticle suspension was bubbled for 3 minutes with H_2 or N_2 at 200 cm^3 min^{-1} after every 10 minutes interval. Figure 6.1 show that the Pt nanoparticle agglomerates are only meta-stable in 20 mM $NaNO_3$ in the presence of H_2 within 30 minutes. The decrease in the UV/vis plasmon adsorption peak is show to be the largest after each period of bubbling, suggesting that mechanical mixing from the flow of H_2 into the nanoparticle suspension contributes significantly to the agglomeration process. To reduce the effect of agglomeration on results, all experiments were performed within 30 minutes following the addition of electrolyte to the nanoparticle solution.

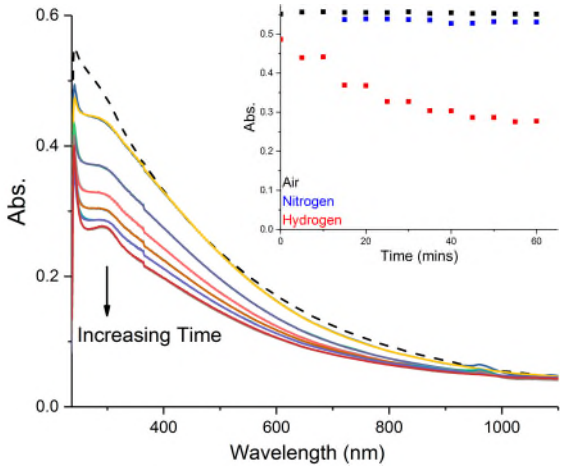

Figure 6.1 UV/vis spectrum of the nominally sized 30 nm Pt nanoparticle aggregates in 20 mM $NaNO_3$ with H_2. Inlay: a plot of the maximum absorption wavelength against the experimental time. The blue, black and red squares represent the Pt nanoparticle aggregates in 20 mM $NaNO_3$ with N_2, Air and H_2 respectively, all at 200 $cm^3 min^{-1}$. The dashed UV/vis curve and the absorbance at 0 mins in all three situations in the inlay are data collected in 20 mM $NaNO_3$ with air, before bubbling with N_2 or H_2. Mass concentration for all particles is 0.026 mg/mL.

References

1. E. W. Weisstein, "Cumulative Frequency." From MathWorld--A Wolfram Web Resource. , http://mathworld.wolfram.com/CumulativeFrequency.html).
2. B. D. A. Levin, Y. Jiang, E. Padgett, S. Waldon, C. Quammen, C. Harris, U. Ayachit, M. Hanwell, P. Ercius, D. A. Muller and R. Hovden, *Microscopy Today*, 2018, **26**, 12-17.
3. B. Goris, W. Van den Broek, K. J. Batenburg, H. H. Mezerji and S. Bals, *Ultramicroscopy*, 2012, **113**, 120-130.
4. J. Canny, in *Readings in computer vision*, Elsevier, 1987, pp. 184-203.
5. J. A. Anderson, C. D. Lorenz and A. Travesset, *Journal of computational physics*, 2008, **227**, 5342-5359.
6. J. Glaser, T. D. Nguyen, J. A. Anderson, P. Lui, F. Spiga, J. A. Millan, D. C. Morse and S. C. Glotzer, *Comput. Phys. Commun.*, 2015, **192**, 97-107.
7. J. A. Anderson, M. E. Irrgang and S. C. Glotzer, *Comput. Phys. Commun.*, 2016, **204**, 21-30.
8. C. Ophus, *Advanced structural and chemical imaging*, 2017, **3**, 13.
9. A. Pryor, C. Ophus and J. Miao, *Advanced structural and chemical imaging*, 2017, **3**, 15.
10. X. Jiao, C. Batchelor-McAuley, C. Lin, E. Kätelhön, E. E. L. Tanner, N. P. Young and R. G. Compton, *ACS Catalysis*, 2018, **8**, 6192-6202.
11. S. Trasatti and O. A. Petrii, *Pure Appl. Chem.*, 1991, **63**, 711-734.
12. X. Jiao, C. Batchelor-McAuley, N. P. Young and R. G. Compton, *PCCP*, 2018, **20**, 23847-23850.